J Mater Sci (2009) 44:6484–6489
DOI 10.1007/s10853-009-3578-5

MESOSTRUCTURED MATERIALS

Synthesis and characterization of TiO_2-incorporated silica foams

H. N. Wang · P. Yuan · L. Zhou · Y. N. Guo · J. Zou · A. M. Yu · G. Q. Lu · C. Z. Yu

Received: 30 November 2008 / Accepted: 12 May 2009 / Published online: 27 May 2009
© Springer Science+Business Media, LLC 2009

Abstract Titania-incorporated silica (TiO_2–SiO_2) porous materials have great applications in diverse areas. In this work, TiO_2–SiO_2 porous materials with tunable Si/Ti molar ratio (R) have been successfully prepared through a one-pot method under a near-neutral condition. With decreasing Si/Ti R, a phase transition from a macroporous foam-like structure to mesostructure is observed. The resultant TiO_2–SiO_2 porous materials possess large surface areas and high pore volumes. In addition, the titania species are homogenously dispersed in silica matrix when Si/Ti $R \geq 10$. Our contribution provides a convenient method to synthesize TiO_2/SiO_2 porous materials with very large pore size, high pore volume, and relatively high titania content well dispersed in the silica wall framework.

Introduction

Titania-incorporated silica (TiO_2–SiO_2) porous materials have great applications as catalysts due to the activity contributed by titanium species and large surface area as well as high pore volume originated from porous structures [1–3]. Since the discovery of mesoporous silica M-41S [4], various TiO_2–SiO_2 porous materials with ordered 2-dimensional (2-D) or 3-dimensional (3-D) mesostructures have been synthesized, such as Ti-MCM-41 [5–8], Ti-MCM-48 [9–12], Ti-SBA-15 [13, 14], and Ti-SBA-1 [15], etc. Recent progresses mainly focus on the synthesis of TiO_2–SiO_2 composites with pore sizes in the mesopore range (2–50 nm), while less attention has been paid to the synthesis of macroporous (pore diameter > 50 nm) TiO_2–SiO_2 materials. It is anticipated that macroporous TiO_2–SiO_2 materials may have wide applications [16, 17] where very large molecules and their reactions occur within the macropores.

TiO_2–SiO_2 porous materials can be synthesized by directly introducing TiO_2 species into silica framework through a hydrolysis–condensation process. However, the hydrolysis rate of TiO_2 precursors [such as titanium butoxide, $Ti(OBu)_4$] is generally faster than that of silica precursors, thus leading to non-homogenous deposition of titania species onto porous silica walls. To avoid this phenomenon, it is necessary to introduce a chelating agent to reduce the hydrolysis rate of TiO_2 precursors to achieve porous materials with homogeneous wall compositions [18].

In the present study, we report a facile approach to synthesize TiO_2–SiO_2 porous materials with tunable Si/Ti molar ratio (R) under slightly acidic conditions. With decreasing Si/Ti R, a phase transition from a macroporous foam-like structure to mesostructure is observed. The resultant TiO_2–SiO_2 porous materials possess large surface areas and high pore volumes. In addition, the titania species can be homogenously dispersed in silica matrix when Si/Ti $R \geq 10$. The TiO_2/SiO_2 porous materials with adjustable

H. N. Wang · P. Yuan · L. Zhou · C. Z. Yu (✉)
Department of Chemistry and Shanghai Key Laboratory of Molecular Catalysis and Innovative Materials, Fudan University, Shanghai 200433, People's Republic of China
e-mail: czyu@fudan.edu.cn

Y. N. Guo · J. Zou
School of Engineering and Centre for Microscopy and Microanalysis, The University of Queensland, St Lucia QLD 4072, Australia

A. M. Yu · G. Q. Lu (✉)
ARC Centre of Excellence for Functional Nanomaterials, School of Engineering and Australian Institute for Bioengineering and Nanotechnology, The University of Queensland, Brisbane, Australia
e-mail: maxlu@uq.edu.au

Si/Ti *R* have been systematically investigated by powder X-ray diffraction (XRD), nitrogen adsorption/desorption, diffuse reflectance UV–Visible (UV–Vis), scanning electron microscopy (SEM), transmission electron microscopy (TEM), and energy dispersive X-ray (EDX) analysis.

Experimental section

Synthesis of TiO_2-incorporated porous silica

The methods for the preparation of TiO_2-incorporated porous silica materials are similar to previous reports [19–21]. TiO_2/SiO_2 porous materials with adjustable Si/Ti *R* were prepared under a near-neutral condition in the presence of a triblock copolymer $EO_{20}PO_{70}EO_{20}$ [denoted P123, BASF, where EO is poly(ethylene oxide) and PO represents poly(propylene oxide)] as the structure-directing agent, tetramethyl orthosilicate (TMOS) as a silica source, Ti(*n*-OBu)$_4$ as a titania source. Acetylacetone (acac) was used as chelating agent to reduce the hydrolysis rate of Ti(*n*-OBu)$_4$. In a typical synthesis procedure, 1.6 g of P123 and 1.7 g of Na_2SO_4 (0.40 M) were dissolved in 30 g of pH = 5.0 NaAc-HAc buffer solution (Ct = 0.02 M, where $Ct = C_{NaAc} + C_{HAc}$) at 35 °C to form a homogenous solution under stirring. To this mixture solution, 1.52 g of TMOS (0.01 mol), desired amounts of Ti(*n*-OBu)$_4$, and acac were added under stirring. The added amount of Ti(*n*-OBu)$_4$ was calculated by Si/Ti *R* (*R* = 50, 40, 30, 20, 10, and 5 in six experiments), while the molar ratio of acac to Ti(*n*-OBu)$_4$ was kept at 2 in six experiments. The stirring was stopped after 5 min and the resultant mixture was kept at a static condition for 24 h and then hydrothermally treated at 100 °C for another 24 h. The precipitates were filtered, washed three times with water to remove inorganic salts, and then dried at room temperature. The final products were obtained by calcination at 550 °C for 5 h.

Characterization

XRD patterns were recorded using Bruker D4 Powder X-ray diffractometer using Cu Ka radiation (40 kV, 40 mA). The step size and step time for small-angle and wide-angle XRD measurement is 0.02° and 0.2 s per step in the range $0.5° < 2\theta < 3°$, 0.05° and 0.2 s per step in the range $5° < 2\theta < 60°$, respectively.

The textural properties of porous materials were evaluated using nitrogen adsorption/desorption measurements with a Quantachrome's Quadrasorb SI analyzer. Nitrogen adsorption/desorption isotherms were measured at 77 K after samples were degassed below 10^{-3} Torr at 473 K for 5 h. The BET surface area was calculated using adsorption data in a relative pressure range from 0.05 to 0.3. The pore-size distribution curves were obtained from analysis of the adsorption branch by the Barrett–Joyner–Halenda (BJH) method.

The UV–Vis spectra were measured with a Cary 5 UV–Vis–NIR spectrophotometer equipped with the Varian diffuse reflectance attachment. Spectra were collected in the wavelength range from 190 to 600 nm. SEM images were taken with a Philips XL30 electron microscope operating at 20 kV. TEM images were obtained with FEI TECNAI 12 operated at 120 kV. Samples for TEM measurements were suspended in ethanol and supported on micro-grids. EDX was attached to the TEM independently, and each data was the average of 10 pots.

Results and discussion

Figure 1 presents the SEM images of calcined TiO_2/SiO_2 porous materials with a series of Si/Ti *R*. When Si/Ti *R* is in the range of 50–30 (Fig. 1a–c), macroporous foam-like structures can be directly observed. The pore sizes are estimated to be ~100 nm, but the pore structures are less ordered compared to pure siliceous foams reported previously [19]. When Si/Ti *R* is decreased to 20 (Fig. 1d), the foam-like structure is less resolved by SEM observation, the size and density of macropores become smaller compared to samples obtained at higher Si/Ti *R*. When the Si/Ti *R* is further decreased to 10 and 5 (Fig. 1e and f, respectively), huge changes in morphology and structure can be observed. Compared to samples obtained at Si/Ti *R* in the range of 50–20, aggregated particles with relatively smaller particle sizes are observed; moreover, the macroporous foam-like structure cannot be directly observed by SEM images, indicating a dramatical structure transformation when Si/Ti *R* is decreased to 10 and 5.

Figure 2 shows TEM images of calcined TiO_2/SiO_2 porous materials synthesized at different Si/Ti *R* demonstrating the representative structures. For porous materials obtained at Si/Ti *R* of 50 and 30 (Fig. 2a and b, respectively), typical foam-like structures fused from vesicles can be observed, which are similar to pure siliceous foams; however, the ordering of packing structures is decreased with the introduction of titania into the silica framework [19, 21]. Because the structures of samples obtained at Si/Ti *R* equal to 30 and 40 are very similar, the TEM image of sample obtained at Si/Ti *R* = 40 is not shown.

When Si/Ti *R* is decreased to 20, the structures changed from uni-lamellar foams to multi-lamellar ones (Fig. 2c), and a small fraction of disordered mesostructures can also be observed in the TEM image. Interestingly, when Si/Ti *R* is 10, a very small fraction of locally ordered mesostructure can be observed together with the multi-lamellar vesicles (indicated by a white arrow) as shown in Fig. 2d. When

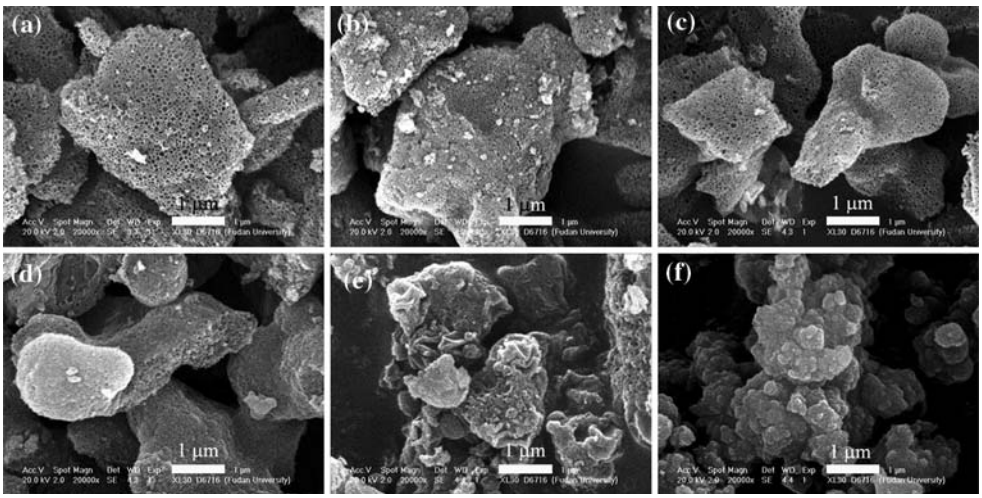

Fig. 1 SEM images (**a**–**f**) of TiO_2–SiO_2 porous materials obtained at Si/Ti $R = 50$, 40, 30, 20, 10, 5, respectively

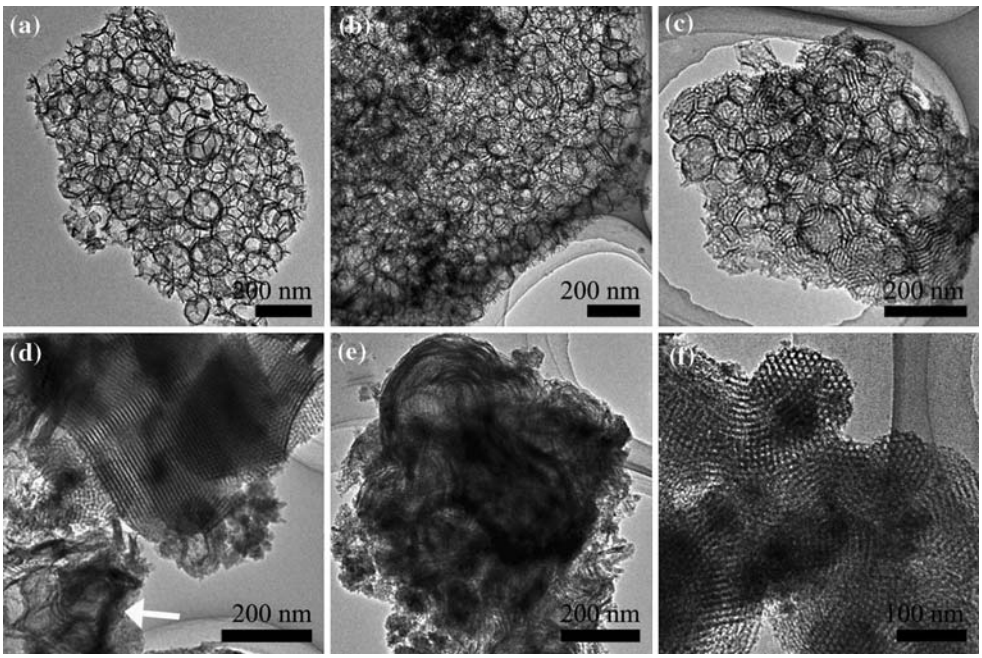

Fig. 2 TEM images (**a**–**f**) of TiO_2–SiO_2 porous materials obtained at Si/Ti $R = 50$ (**a**), 30 (**b**), 20 (**c**), 10 (**d**), 5 (**e** and **f**), respectively

finally increasing Si/Ti R to 5, TEM images show again a mixture of multi-lamellar vesicles and hexagonal mesostructure (Fig. 2e and f, respectively). The observed domains of hexagonal structure are greatly increased compared to sample prepared at a Si/Ti R of 10. The average d-spacing of multilayer vesicles is estimated to be 7 nm (Fig. 2e) while the distance between two adjacent channels (d_{10}) is measured to be 10 nm in the ordered hexagonal domain (Fig. 2f).

Figure 3 shows the small angle XRD patterns of calcined TiO_2/SiO_2 porous materials obtained at different Si/Ti R. XRD patterns of samples obtained at Si/Ti R in the range of 50–10 show no diffraction peaks in the small angle region. However, for the sample prepared at the smallest Si/Ti R of 5, a broad diffraction peak before $2\theta = 1°$ can be detected, indicating the existence of a significant fraction of ordered domains. The small angle XRD observation agrees well with TEM result (Fig. 2f), that is, a considerable fraction of hexagonal mesostructures coexist with multi-lamellar vesicles.

Figure 4 gives the adsorption–desorption isotherms of calcined TiO_2/SiO_2 composites. Porous materials prepared at Si/Ti $R = 50$, 40, and 30 show typical type II isotherms, relatively large hysteresis loops, and capillary condensation steps at relative pressure $(P/P_0) > 0.8$. With further decreasing Si/Ti R, the isotherms gradually changed from

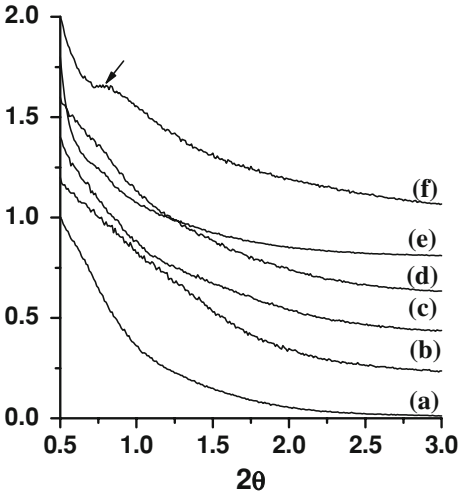

Fig. 3 Small-angle XRD patterns (a–f) of calcined TiO_2–SiO_2 porous materials obtained at Si/Ti $R = 50$, 40, 30, 20, 10, and 5, respectively

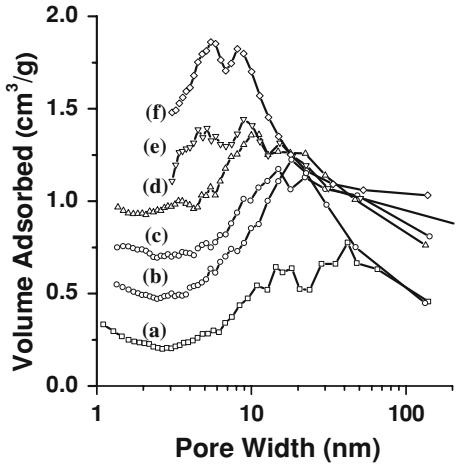

Fig. 5 Pore size distribution curves (a–f) of calcined TiO_2–SiO_2 porous materials obtained at Si/Ti $R = 50$, 40, 30, 20, 10, and 5, respectively. The Y-axes value is raised 0.2, 0.4, 0.6, 0.8, and 1.0 cm^3/g for curves b, c, d, e, and f, respectively

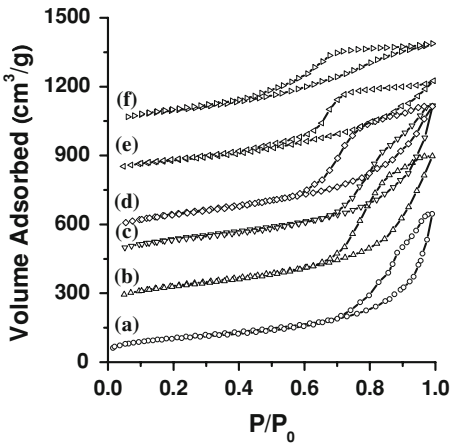

Fig. 4 N_2 adsorption–desorption isotherms (a–f) of calcined TiO_2–SiO_2 porous materials obtained at Si/Ti $R = 50$, 40, 30, 20, 10, and 5, respectively. The Y-axes value is 200, 400, 600, 800, and 1000 g cm^3/g higher for isotherms b, c, d, e, and f, respectively

type II to type IV, and the capillary condensation steps moves to relatively lower P/P_0, indicating that the pore size is decreased. The pore size distribution curves of calcined TiO_2/SiO_2 porous materials prepared at different Si/Ti R are shown in Fig. 5. It is noteworthy that for samples obtained at higher titania contents (Si/Ti $R = 10$ and 5), a typical bimodal pore size distribution pattern can be seen with the first and second peaks located at 5.8 and 8.6 nm, respectively. Combining the TEM results, these two peaks should be attributed to the spacing between the layers of multi-lamellar vesicles and diameters of hexagonally arrayed mesopores, respectively. The pore volume and surface area of porous materials synthesized in this study are summarized in Table 1. It can be seen that all samples

Table 1 Physicochemical properties of TiO_2–SiO_2 porous materials obtained at Si/Ti R and pH measured before hydrothermal treatment

Si/Ti R^a	Si/Ti R^b	V (cm^3/g)	S (m^2/g)	pH[c]
50/1	75.02	1.00	369	4.8
40/1	48.60	1.08	474	4.7
30/1	45.48	1.11	487	4.7
20/1	27.43	0.95	517	4.5
10/1	16.50	0.66	295	4.2
5/1	7.300	0.60	362	3.8

V pore volume, S BET surface area

[a] The initial Si/Ti R during synthesis

[b] Si/Ti R determined from EDX

[c] The pH value measured before hydrothermal treatment

with foam-like structures (Si/Ti R in the range of 50–30) have relatively large pore volumes (>1.0 cm^3/g). When the hexagonal mesostructure is partially formed (Si/Ti R of 10 and 5), the pore volumes of resultant materials are greatly reduced.

Figure 6 shows the wide-angle XRD patterns of calcined TiO_2/SiO_2 porous materials synthesized at different Si/Ti R. For samples prepared at Si/Ti $R = 50$–10 (Fig. 6a–e, respectively), only one broad peak located at $2\theta = 22°$ is observed, which is corresponded to amorphous SiO_2. For the wide-angle XRD pattern of sample obtained at a Si/Ti R of 5, one more diffraction peak at $2\theta \sim 25°$ is observed, indicating a small amount of bulk anatase exists in the amorphous silica [22, 23].

The distribution of titania species in silica matrix is characterized by UV–Vis diffuse reflectance spectroscopy (Fig. 7), which is an extensively used technique to detect

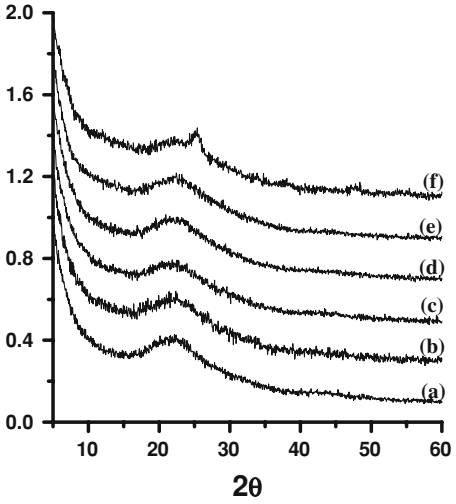

Fig. 6 Wide-angle XRD pattern (a–f) of calcined TiO_2–SiO_2 porous materials obtained at Si/Ti $R = 50$, 40, 30, 20, 10, and 5, respectively

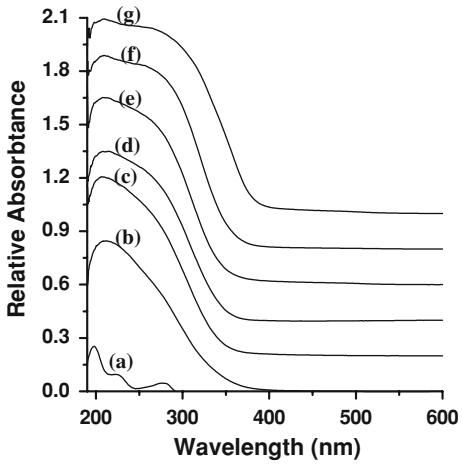

Fig. 7 UV–vis spectra (a) of pure silica oxide, (b–f) of calcined TiO_2–SiO_2 porous materials obtained at Si/Ti $R = 50$, 40, 30, 20, 10, and 5, respectively

the framework and extra-framework of titanium species [24]. As can be seen from Fig. 7, the maximum absorption band is observed at about 210 nm for all samples synthesized at Si/Ti R of 50–5, which can be attributed to the charge-transfer from the ligand oxygen to an unoccupied orbital of the central titanium ion in well dispersed framework [TiO_4] or [$HOTiO_3$] units [24]. Moreover, another absorption can be observed at 265 nm, which comes from low-energy charge-transfer transition between tetrahedral oxygen ligands and central Ti^{4+} of dispersed titanium species in frameworks [25]. In addition, by comparing the relative intensity of two peaks centered at 210 and 265 nm, it can be seen that the intensity of the peak located at 265 nm increases monotonically with Si/Ti R decreasing, in accordance with previous report [24]. It is noted that the maximum absorption characteristic for aggregated titania particles (anatase phase) occurs at 330 nm [19]. The absence of such a band at 330 nm indicates that no bulk anatase TiO_2 is produced in samples obtained at Si/Ti $R = 50$–10; thus, all titanium species are distributed homogeneously within the wall frameworks. For the sample obtained at Ti/Si R of 5, a small amount of bulk anatase is detected by XRD, the UV–Vis diffuse reflectance spectra also indicates the existence of small TiO_2 clusters [22] in the final composite.

By comparing the bulk Si/Ti R (calculated from reagents) and measured Si/Ti R in calcined TiO_2/SiO_2 porous materials in our synthesis (Table 1), it can be seen that the Si/Ti R in the final product is close to that in the initial recipe, suggesting that the leaching of titania species is not a big concern in our synthesis approach under mild pH. Furthermore, by comparing the UV–Vis diffuse reflectance spectra of TiO_2/SiO_2 porous materials with the same Si/Ti R ($R = 5$) synthesized in literature [24] and our own study, it can be seen that our method is advantageous for a successful isomorphous substitution of titanium inside the siliceous framework while avoiding the formation of bulk anatase phases. In addition, the use of acac in our synthesis is not only helpful in controlling the hydrolysis and condensation of titania species to form homogeneously distributed composite materials, but also leading to a pH change in the reaction solution. The pH of initial buffer solution before reaction is 5.0, after the reaction (measured before hydrothermal treatment), the pH value of solution decreases as the Si/Ti R decreases (Table 1), which can be explained by the increasing amount of H^+ released due to the chelation between acac and Ti (IV) because the molar ratio of acac/Ti was kept as a constant in our synthesis. With decreasing pH at decreasing Si/Ti R, the hydrolysis rate of TMOS can be accelerated. At the same time, the relative stronger protonation of EO groups may increase the hydrophilic–hydrophobic ratio of organic/inorganic composites, thus leading to a structural transformation from foam-like structure [19–21] to hexagonal mesostructure as reported in pure siliceous systems [26–28].

Conclusions

In conclusion, TiO_2–SiO_2 porous materials with tunable Si/Ti R have been successfully prepared through a simple, one-pot method. With decreasing Si/Ti R, a phase transition from macroporous foam-like structure to mesostructure is observed. The resultant TiO_2–SiO_2 porous materials possess large surface areas and high pore volumes. In addition, the titania species can be homogenously dispersed in silica matrix when Si/Ti $R \geq 10$. Our contribution provides a convenient method to synthesize TiO_2/SiO_2 porous

materials with very large pore size, high pore volume, and relatively high titania content well dispersed in the silica wall framework. Such functional materials are expected to find applications in catalysis, enzymatic digestion of proteins, and in the enrichment of phosphopeptides for proteomic research.

Acknowledgements This work is supported by the State Key Research Program (2004CB217800), Science & Technology Commission of Shanghai Municipality (08DZ2270500), SLADP (B113), CNSF (20721063), Shanghai Science Committee (07QH14003), NCET, the Ministry of Education of China (20060246010), and the Australian Research Council.

References

1. Corma A (1997) Chem Rev 97:2373
2. Kholdeeva OA, Trukhan NN (2006) Russ Chem Rev 75:411
3. Orlov A, Zhai QZ, Klinowski J (2006) J Mater Sci 41:2187. doi: 10.1007/s10853-006-7184-5
4. Kresge CT, Leonowicz ME, Roth WJ, Vartuli JC, Beck JS (1992) Nature 359:710
5. Anpo M, Yamashita H, Ikeue K, Fujii Y, Zhang SG, Ichihashi Y, Park DR, Suzuki Y, Koyano K, Tatsumi T (1998) Catal Today 44:327
6. Corma A, Navarro MT, Pariente JP (1994) J Chem Soc Chem Commun 147
7. Maschmeyer T, Rey F, Sankar G, Thomas JM (1995) Nature 378:159
8. Yu JQ, Feng ZC, Xu L, Li MJ, Xin Q, Liu ZM, Li C (2001) Chem Mater 13:994
9. Morey M, Davidson A, Stucky G (1996) Microporous Mater 6:99
10. Morey MS, Davidson A, Stucky GD (1998) J Porous Mater 5:195
11. Morey MS, O'Brien S, Schwarz S, Stucky GD (2000) Chem Mater 12:898
12. Koyano KA, Tatsumi T (1996) Chem Commun 145
13. Luan ZH, Maes EM, van der Heide PAW, Zhao DY, Czernuszewicz RS, Kevan L (1999) Chem Mater 11:3680
14. Zhang WH, Lu JQ, Han B, Li MJ, Xiu JH, Ying PL, Li C (2002) Chem Mater 14:3413
15. Ji D, Zhao R, Lv GM, Qian G, Yan L, Suo JS (2005) Appl Catal A Gen 281:39
16. Johnson BJS, Stein A (2001) Inorg Chem 40:801
17. Liang H, Zhang Y, Liu Y (2008) J Nat Gas Chem 17:403
18. Brinker CJ, Scherer GW (1990) The physics and chemistry of sol-gel processing sol-gel science. Academic Press, San Diego, CA
19. Wang HN, Zhou XF, Yu MH, Wang YH, Han L, Zhang J, Yuan P, Auchterlonie G, Zou J, Yu CZ (2006) J Am Chem Soc 128:15992
20. Yuan P, Zhou XF, Wang HN, Liu N, Hu YF, Auchterlonie G, Drennan J, Yao XD, Lu GQ, Zou J, Yu CZ (2009) Small 5:377
21. Wang HN, Wang YH, Zhou XF, Zhou L, Tang JW, Lei J, Yu CZ (2007) Adv Funct Mater 17:613
22. Berube F, Kleitz F, Kaliaguine S (2008) J Phys Chem C 112:14403
23. Alba MD, Luan ZH, Klinowski J (1996) J Phys Chem 100:2178
24. Vayssilov GN (1997) Catal Rev Sci Eng 39:209
25. Luan ZH, Kevan L (1997) J Phys Chem B 101:2020
26. Kim JM, Sakamoto Y, Hwang YK, Kwon YU, Terasaki O, Park SE, Stucky GD (2002) J Phys Chem B 106:2552
27. Hsu YC, Chang YH, Yang CM (2008) Adv Funct Mater 18:1799
28. Liu J, Zhang L, Yang QH, Li C (2008) Microporous Mesoporous Mater 116:330